The architectural application of shells whose boundaries subtend a constant solid angle

Comput. Aided Geom. Des. 111 (2024) 102331

Contents lists available at ScienceDirect

Computer Aided Geometric Design

journal homepage: www.elsevier.com/locate/cagd

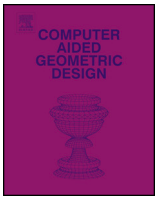

The architectural application of shells whose boundaries subtend a constant solid angle ☆

Emil Adiels *, Mats Ander, Chris J.K. Williams

Department of Architecture and Civil Engineering, Chalmers University of Technology, SE-412 96 Gothenburg, Sweden

ARTICLE INFO

Keywords:
Differential geometry
Architectural geometry
Solid angle
Shells
Form finding
Potential theory

ABSTRACT

Surface geometry plays a central role in the design of bridges, vaults and shells, using various techniques for generating a geometry which aims to balance structural, spatial, aesthetic and construction requirements.

In this paper we propose the use of surfaces defined such that given closed curves subtend a constant solid angle at all points on the surface and form its boundary. Constant solid angle surfaces enable one to control the boundary slope and hence achieve an approximately constant span-to-height ratio as the span varies, making them structurally viable for shell structures. In addition, when the entire surface boundary is in the same plane, the slope of the surface around the boundary is constant and thus follows a principal curvature direction. Such surfaces are suitable for surface grids where planar quadrilaterals meet the surface boundaries. They can also be used as the Airy stress function in the form finding of shells having forces concentrated at the corners.

Our technique employs the Gauss-Bonnet theorem to calculate the solid angle of a point in space and Newton's method to move the point onto the constant solid angle surface. We use the Biot-Savart law to find the gradient of the solid angle. The technique can be applied in parallel to each surface point without an initial mesh, opening up for future studies and other applications when boundary curves are known but the initial topology is unknown.

We show the geometrical properties, possibilities and limitations of surfaces of constant solid angle using examples in three dimensions.

1. Introduction

Architectural geometry is the application of geometry to the design and construction of buildings and bridges, particularly those with curved surfaces like shells and grid shells (Figs. 1(a) and (b)). The surface curvature enables the shell to carry load mainly through membrane action, making them much more material efficient than conventional flat slabs and beams. The complex geometry, combined with requirements and desires regarding economic, structural, production, spatial and aesthetic aspects, makes this a topic that has fascinated builders and mathematicians for centuries. Early treatises in architectural geometry include *Le premier tome de l'architecture* by Philibert de Lorme (1512-1570), examining the art of cutting stones in vaults, while an extensive overview of

☆ Editor: Johannes Wallner.

* Corresponding author.
E-mail address: emil.adiels@chalmers.se (E. Adiels).

https://doi.org/10.1016/j.cagd.2024.102331
Received 11 October 2022; Received in revised form 25 April 2024; Accepted 28 April 2024

Available online 3 May 2024

Fig. 1. (a) The British Museum Great Court roof, by Foster and partners, Buro Happold and Waagner Biro. Photo by Andrew Stawarz, licensed under CC BY-ND 2.0. (b) Grid shell of the Hippo House by Schlaich Bergermann partner, photo used with permission © Zoo Berlin.

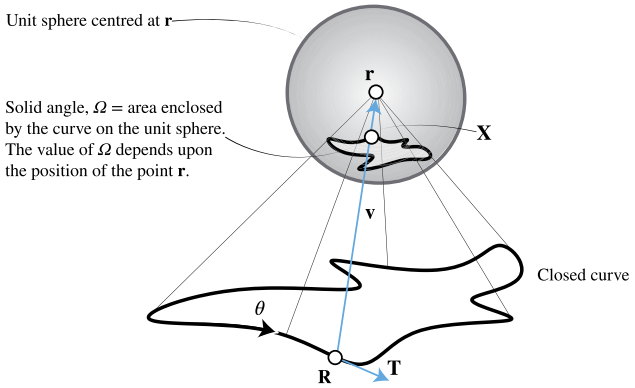

Fig. 2. Solid angle Ω subtended at a point $\mathbf{r}$ is the surface area enclosed by the curve on the unit sphere. $\mathbf{R}$ is a typical point on the boundary, which is a function of curve parameter θ, where $\mathbf{T}$ is the tangent. Vector $\mathbf{v}$ goes from $\mathbf{R}$ to $\mathbf{r}$ and cuts the unit sphere at the point $\mathbf{X}$. $\mathbf{R}$, $\mathbf{r}$ and $\mathbf{X}$ are position vectors relative to some fixed origin.

contemporary techniques and applications from the field of differential geometry can be found in Pottmann et al. (2014). Meanwhile, shell designers have experimented with various shapes to balance requirements and qualities, like ruled surfaces by Antoni Gaudí (Collins, 1963; Huerta, 2006) and Félix Candela (Faber, 1963), Eladio Dieste's "Gaussian vaults" (Allen, 2003), and translational surfaces (Fig. 1(b)) by Jörg Schlaich (Schlaich and Schober, 1996). Other examples include Weingarten surfaces (Pellis et al., 2021), such as surfaces of revolution and constant mean curvature surfaces, which include minimal surfaces. Additional techniques include form finding (Adriaenssens et al., 2014) striving for structural efficiency or a specific state of stress for a given load. Examples include minimising surface tension, bending energy or strain energy producing soap films (Klaus et al., 1987), Willmore energy surfaces (Williams, 1987) or hanging nets (Rubió i Bellver, 1913).

We propose an alternative using surfaces defined by points which all have the same constant solid angle, subtended by a given curve. The solid angle Ω is defined in Fig. 2 (Van Oosterom and Strackee, 1983; Weisstein, n.d.) and for a fixed curve the solid angle is a function of point $\mathbf{r}$ in the centre of the unit sphere, and so our surface is defined by

$$\Omega = \Omega(\mathbf{r}) = \text{constant}.$$

Thus we have a scalar Ω which is a function of $\mathbf{r}$, as $\mathbf{r}$ changes the unit sphere whose centre is $\mathbf{r}$ also moves. We require an isosurface of a scalar field and therefore we could use techniques such as marching cubes (Lorensen and Cline, 1987). However, we are able to calculate Ω and also its gradient $\nabla\Omega$ at any point $\mathbf{r}$ and so we can use Newton's method to find the points on the isosurface with a high degree of accuracy. Thus we have the equation

$$\mathbf{r}_{n+1} = \mathbf{r}_n - \left(\Omega_n - \Omega_c\right) \frac{(\nabla\Omega)_n}{|\nabla\Omega|_n^2} \tag{1}$$

in which Ω_c is our constant value of Ω and n is the iteration number in Newton's method. The process is described in Fig. 3 and §3 where we explain the use of the $(\nabla\Omega)_n / |\nabla\Omega|_n^2$.

The benefit of constant solid angle surfaces is that they enable one to control the boundary slope and hence achieve an approximately constant span-to-height ratio as the span varies. This is because solid angle is dimensionless and is therefore scale

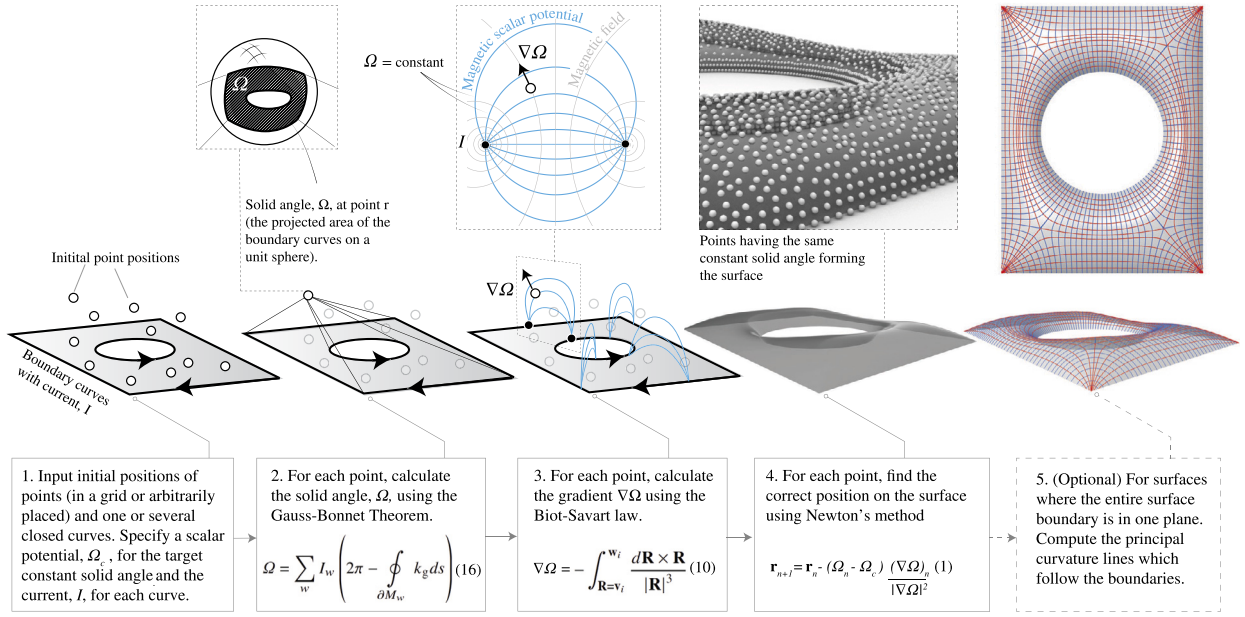

Fig. 3. The steps of our method for generating surfaces of constant solid angle. The first four steps are necessary while the last step is optional and specifically interesting for surfaces where the entire boundary is in the same plane.

independent. Alternative techniques such as constant mean curvature surfaces, which are equivalent to an inflated soap film, depend upon quantities with dimensions. These properties of solid angle surfaces make them structurally viable for shells and grid shells, even though the formulation takes no regard of structural aspects. For cases where the entire boundary is in the same plane, the slope is constant along its boundaries. This means the surface boundary follows a principal curvature direction, which is an otherwise rare occurrence. Therefore, solid angle surfaces are suitable for situations when surface grids of planar quadrilaterals are desired for economic or production requirements since the panels are not cut at the boundary, which usually is an unfortunate consequence of these patterns as seen in Fig. 1(b). Another potential application for surfaces having constant slope along the surface boundary is as Airy stress functions, ϕ, which can be used in Pucher's equation (Timoshenko and Woinowsky-Krieger, 1959) for form finding of shells as done by Miki et al. (2015, 2022). Such an Airy stress function would result in a shell where the lateral thrust is concentrated to the corners.

Our technique for generating these surfaces is simple and straightforward since it does not necessarily require any initial mesh, such as many form finding techniques used in architecture, for example dynamic relaxation (Adriaenssens et al., 2014) or force density method (Schek, 1974). Each point can find itself onto the surface independently meaning the process can be done in parallel on a GPU. It opens up a third application for this type of surfaces beyond architecture in for instance industrial design or computer graphics. Having only known boundaries one can find a surface using this technique without having an initial mesh.

The method, illustrated in Fig. 3, at minimum, requires the designer to input one closed boundary curve with a chosen strength and direction of the current, a scalar potential for the constant solid angle, and a number of points that can be positioned in a grid or arbitrarily placed. Based on the inputs from the designer there are then three more steps. First, we calculate the solid angle using the Gauss-Bonnet theorem, §4. Secondly, we find the gradient, which is also the surface normal, using the Biot-Savart law, §6. Lastly, we use Newton's method to move the points to the surface, §3. Examples of various surfaces can be found in §9. The technique we present is for generating the surface itself, which is the main focus of this paper. However, it can be expanded to include the generation of surface grids such as principal curvature nets, Chebyshev nets, and geodesic coordinates. Optionally, such grids can be applied afterwards on the generated surface. In §7 we show two methods to compute the curvature and principal curvature directions, which can be used to generate a principal curvature net.

1.1. Connection between the shell form and the shell pattern

The surface and its surface pattern of triangles or quadrilaterals are connected through the components of the first and the second fundamental form (Struik, 1961; Stoker, 1969; Green and Zerna, 1968). From a structural point of view, a triangular grid might be more desirable than a quadrilateral grid (Wright, 1965), but from a production point of view, a quadrilateral grid may be preferable as described by Schlaich and Schober (2005).

There are three compatibility equations, the Gauss-Codazzi equations, connecting the six components of the first and second fundamental form, which tell us how a grid on a surface has to be deformed to cover a doubly curved surface. If the surface can be considered to be acting as a membrane shell there are three components of the stress tensor and three equations of static equilibrium

(Green and Zerna, 1968). Meaning there are, in total, nine unknowns and six equations requiring the designer to introduce three more equations or constraints, which could be used to facilitate a more economic production. Examples of surface grids include equal mesh Chebyshev nets[1] (Chebyshev, 1946) used for continuous laths in the Mannheim Multihalle (Liddell, 2015), geodesic coordinate nets[2] following the bed joints on masonry shells (Adiels et al., 2017; Adiels and Williams, 2021) or cutting patterns of tensile nets (Williams, 1980), and principal curvature nets, which consist of principal curvature lines intersecting at right angles.

We can find as many points as necessary to produce smooth grids on the surface. However, for a real grid shell there is a finite number of nodes, usually joined by straight members, in which case discrete differential geometry (Crane et al., 2013; Pottmann and Wallner, 2017) can be used to produce planar panels, which will approximate to rectangles if the grid follows the directions of the principal curvatures.

If we have smooth coordinate curves following the principal curvature directions it means that F and f are zero using the notation in Struik (1961) (a_{12} and b_{12} in Green and Zerna (1968)). Work has also been done in aligning the principal stress and principal curvature direction by for instance Tellier et al. (2019) and Pellis and Pottmann (2018). One of the issues with a principal curvature net is that it does not guarantee a nice connection to the boundary, making it necessary to cut the grid, which is usually not good for the architectural expression and requires specially made panels and components. Thus, ideally, one would have a surface such that the principal directions are aligned with the boundaries, meaning a constant slope along the boundary.

1.2. Surfaces exercising boundary slope restrictions

Previous work in controlling the boundary slope has been done using surfaces that minimize the Willmore energy (Bobenko and Schröder, 2005). This is equivalent to minimizing the bending energy and is similar to the shapes we see in cells (Müller and Röger, 2014), but it is also a feature that is beneficial for structural shells and membranes (Williams, 1987).

To find a surface which minimizes the Willmore energy it is necessary to solve a differential equation whereas points on a surface of constant solid angle subtended by the boundary curves but can be found individually and independently for each point. When the surface boundaries are in the same plane the slope along the boundary is constant, a constant one can choose. Surface of constant solid angle appears in potential theory (Lamb, 1932) and can be used for very complicated boundaries (Binysh, 2019; Binysh and Alexander, 2018).

A simpler version of the technique described in this paper was used for the design of the courtyard roofs of the British Museum Great Court (Williams, 2001) (Fig. 1(a)) and Het Scheepvaartmuseum in Amsterdam (Adriaenssens et al., 2012). This simpler version used the reciprocal of the gradient of the solid angle in the horizontal plane to determine the vertical coordinate. In the case of a boundary consisting of two infinite parallel straight lines this would produce a parabolic cross section, rather than the circles shown in Fig. 5.

2. Surfaces of constant solid angle

In §1 we introduced the arbitrary point in space $\mathbf{r}$ which can be joined with straight lines to all the points on a given closed curve to form a ruled surface or cone, but almost invariably without a circular cross-section. This cone will intersect a sphere of arbitrary radius centred at $\mathbf{r}$ with another closed curve and the solid angle, measured in steradians, is the surface area enclosed by the curve on the sphere divided by the square of the radius of the sphere. The sphere is often taken as unit radius, but even so it is important to note that the solid angle is always dimensionless (Fig. 2).

If the curve crosses itself on the unit sphere some areas will be positive and some negative, exactly as in ordinary integration. The surface area of a complete unit sphere is 4π and if Ω is the solid angle subtended by the boundary curve, then $4\pi - \Omega$ is the area on the surface outside the boundary. In the case of a plane boundary, the solid angle is 2π if the apex is in the plane inside the boundary or 0 (or 4π) if it is in the plane outside the boundary. Going around any closed boundary a number of times the solid angle increases or decreases by 4π each revolution and then jumps back again. Being very close to a boundary the change in solid angle is twice the angle of rotation around the boundary, 4π instead of 2π for a complete rotation.

It is now possible to define a *constant solid angle surface* as the locus of points such that one or several given closed curves subtend the same solid angle Ω at all points on the surface, as in Fig. 4. In other words the solid angle subtended by a given boundary curve at point $\mathbf{r}$ depends upon the position of $\mathbf{r}$. If we say that the solid angle should remain constant then $\mathbf{r}$ is constrained to move on a surface. Thus the surface is defined by a potentially infinite number of points and these points can be arranged in any pattern we care to choose on the surface. In Fig. 4 the points were distributed randomly in the plane and then moved onto the surface using the iteration in (1). We could introduce u,v surface coordinates to define a grid on the surface, in which case we need an algorithm to move the points tangential to the surface. This grid could, for example be a Chebyshev net as described above.

[1] Chebyshev nets require constraints $a_{11} = a_{22} = L, n^{12} = 0$ using notation in Green and Zerna (1968).

[2] Geodesic coordinate nets require constraints $a_{22} = L, a_{12} = n^{12} = 0$ using notation in Green and Zerna (1968).

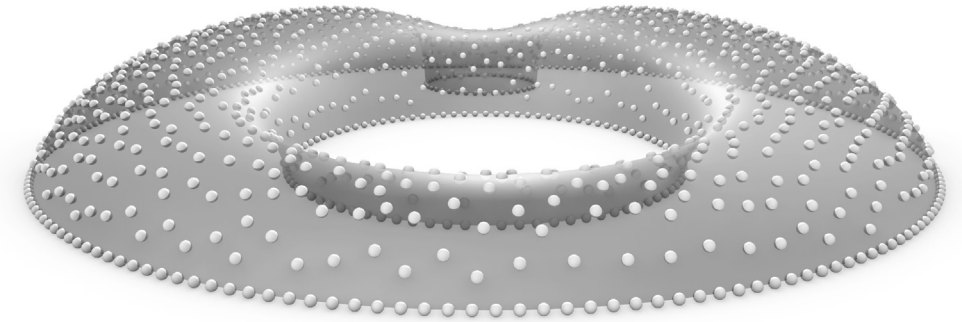

Fig. 4. Points having the same constant solid angle subtended by three circles in the same plane. They all lie on the constant solid angle surface.

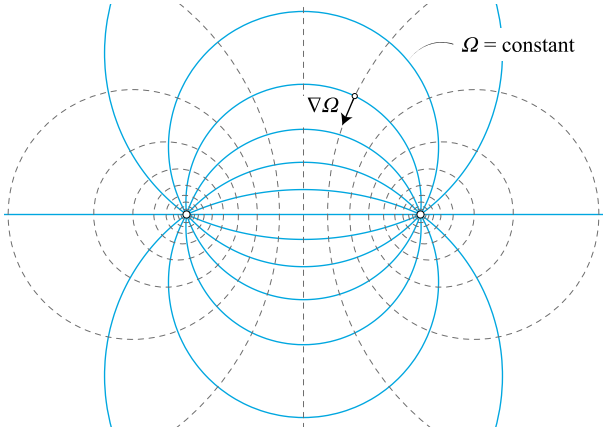

Fig. 5. Section through different level surfaces of constant solid angle and their gradient for the case of a boundary consisting of two infinitely long parallel straight lines. The surfaces are circular cylinders (Lamb, 1932) and correspond to surfaces of constant magnetic scalar potential for the case of a current running along one of the wires and back along the other. They also correspond to the surfaces of constant velocity potential associated with a clockwise and anticlockwise vortex similar to that left behind an aircraft.

As we approach the boundary the gradient of the solid angle is controlled by the local boundary and tends to infinity as the distance from the boundary tends to zero, exactly like approaching a vortex in fluid mechanics or a current-carrying wire in electromagnetic theory. The potential function, in this case the solid angle, remains finite but its gradient tends to infinity. Thus, in the immediate vicinity of the boundary the solid angle varies linearly with rotation around the boundary and for a plane horizontal boundary, the slope of a constant solid angle surface at the boundary is constant and equal to $\pi - \Omega/2$. In addition, as we move around a plane boundary there is no rotation of the normal about an axis tangent to the boundary. The boundary is therefore a principal curvature direction on the surface.

This last point is a special case of Joachimsthal's theorem (Joachimsthal, 1846) where one of the surfaces is the plane of the boundary.

3. Method of finding a constant solid angle surface

In general it is not possible to explicitly calculate the shape of a constant solid angle surface. Even for a circular boundary this requires an elliptic integral (Sadowsky and Sternberg, 1950). However, we shall see that it is possible to calculate the solid angle Ω subtended by the boundary at any given point in space by approximating the boundary to a series of short straight lines. We can also calculate the gradient of the solid angle $\nabla\Omega$ which tells us how the solid angle varies if we move slightly.

Let us imagine that Ω_c is the constant value of solid angle on the surface we wish to generate. If we start at an arbitrary point in space $\mathbf{r}_n$ we can calculate the solid angle Ω_n and its gradient $(\nabla\Omega)_n$ at that point.

We can now move to a new point $\mathbf{r}_{n+1}$ given by (1) which will be nearer to the surface. We can expect to have to do this a number of times, but once we are near the surface it will converge rapidly. This is an application of Newton's method, which is usually written

$$x_{n+1} = x_n - \frac{f(x_n)}{f'(x_n)}$$

for the solution of

$$f(x) = 0.$$

Newton's method also applies when x is a vector and f is a scalar as in our case, where we replace $1/f'$ by $(\nabla\Omega)_n / |\nabla\Omega|_n^2$. Newton's method is often used in non-linear structural analysis when f' is replaced by the tangent stiffness matrix so that $1/f'$ is replaced by the inverse of the tangent stiffness matrix (Zienkiewicz and Taylor, 1991). As always with Newton's method we have to be careful when the gradient is small in case we jump much too far, in which case we can multiply the movement in (1) by some factor less than 1.0. This means we can apply a factor less than 1.0 at the beginning of the simulation to avoid hitting the wrong solution, but as the solution starts to converge, we can put it back to 1.0. For example, in Fig. 21 (d), two possible height values satisfy the requirement for a constant solid angle if we specify the positions in the xy-plane. Thus, we must be careful to obtain the proper height value.

The movement in (1) is in the direction of the gradient, normal to a surface of constant Ω. We are, of course, at liberty to also move points tangential to the surface in order to satisfy some requirement of the grid pattern on the surface.

4. Calculation of the solid angle subtended by a closed curve

In order to find a point on a constant solid angle surface we have to be able to calculate the solid angle subtended by the boundary at the point and the gradient of the solid angle at the same point so that we can move the point bit by bit onto the constant solid angle surface using Newton's method.

The Gauss-Bonnet theorem (Struik, 1961; Eisenhart, 1947) enables us to transform the double integral to find the surface area enclosed by the curve on the unit sphere to a line integral,

$$\int_M K\,dA + \oint_{\partial M} k_g\,ds = 2\pi$$

in which dA is an element of area on the region of surface M, which here is on the unit sphere. ∂M is the boundary of the region M with arc length s, K is the Gaussian curvature of the surface, which is 1 on the unit sphere and k_g is the geodesic curvature of the boundary curve on the unit sphere. The geodesic curvature of a curve on a surface is the curvature of the curve as seen when looking at it directly back down the normal to the surface.

Note that the sign of k_g is changed if the direction of travel is reversed around the curve, with a corresponding change to the value of Ω. The direction of travel does not matter as long as it is consistent. However, having a boundary consisting of several closed boundary curves the directions of travel must be coordinated and compatible.

Thus

$$\Omega = 2\pi - \oint_{\partial M} k_g\,ds. \tag{2}$$

In Fig. 2 $\mathbf{R}(\theta)$ is a typical point on the boundary, which is a function of curve parameter θ which may or may not be equal to the arc length. $\mathbf{r}$ is the point in space at which we want to find the solid angle subtended by the boundary and $\mathbf{v}$ is the vector from $\mathbf{R}$ to $\mathbf{r}$.

Vector $\mathbf{v}$ cuts the unit sphere at the point given by the vector $\mathbf{X}$ and $\mathbf{T}$ is the unit tangent to the boundary. Thus, treating $\mathbf{r}$ as a constant, we have

$$\begin{aligned}
\mathbf{R}_{,\theta} &= \frac{d\mathbf{R}}{d\theta} \\
\mathbf{T} &= \frac{\mathbf{R}_{,\theta}}{|\mathbf{R}_{,\theta}|} \\
\mathbf{X} &= \mathbf{r} - \frac{\mathbf{v}}{|\mathbf{v}|} \\
\mathbf{v} &= \mathbf{r} - \mathbf{R} \\
\mathbf{X}_{,\theta} &= -\left(\frac{\mathbf{v}}{|\mathbf{v}|}\right)_{,\theta} = \frac{|\mathbf{R}_{,\theta}|}{|\mathbf{v}|}\left(\mathbf{T} - \frac{(\mathbf{v}\cdot\mathbf{T})\,\mathbf{v}}{|\mathbf{v}|^2}\right) \\
|\mathbf{X}_{,\theta}| &= \frac{|\mathbf{R}_{,\theta}|\,|\mathbf{v}\times\mathbf{T}|}{|\mathbf{v}|^2}.
\end{aligned}$$

$\mathbf{X}_{,\theta}/|\mathbf{X}_{,\theta}|$ is the unit tangent to the curve on the unit sphere and

$$\frac{ds}{d\theta} = |\mathbf{X}_{,\theta}|$$

since s is the arc length of the curve on the unit sphere. Therefore the curvature vector of the curve on the unit sphere is equal to

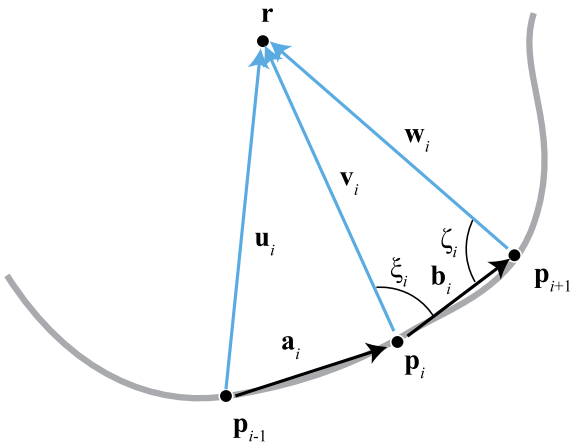

Fig. 6. Three points along the boundary and the point **r** at which to calculate the solid angle.

$$\frac{d}{ds}\left(\frac{\mathbf{X}_{,\theta}}{|\mathbf{X}_{,\theta}|}\right)=\frac{1}{|\mathbf{X}_{,\theta}|}\frac{d}{d\theta}\left(\frac{\mathbf{X}_{,\theta}}{|\mathbf{X}_{,\theta}|}\right).$$

The geodesic curvature is equal to component of this vector perpendicular to the plane containing **v** and **T** so that

$$k_{\mathrm{g}}=\frac{1}{|\mathbf{X}_{,\theta}|}\frac{d}{d\theta}\left(\frac{\mathbf{X}_{,\theta}}{|\mathbf{X}_{,\theta}|}\right)\cdot\frac{(\mathbf{v}\times\mathbf{T})}{|\mathbf{v}\times\mathbf{T}|}=\frac{|\mathbf{v}|\left(\mathbf{T}_{,\theta}\cdot(\mathbf{v}\times\mathbf{T})\right)}{|\mathbf{X}_{,\theta}|\,|\mathbf{v}\times\mathbf{T}|^2}$$

and

$$\Omega=2\pi-\oint\frac{|\mathbf{v}|\left(\mathbf{T}_{,\theta}\cdot(\mathbf{v}\times\mathbf{T})\right)}{|\mathbf{X}_{,\theta}|\,|\mathbf{v}\times\mathbf{T}|^2}ds=2\pi-\oint\frac{|\mathbf{v}|\left(\mathbf{T}_{,\theta}\cdot(\mathbf{v}\times\mathbf{T})\right)}{|\mathbf{v}\times\mathbf{T}|^2}d\theta. \tag{3}$$

As discussed in §3, the integral (3) is difficult to evaluate analytically for even the simplest of geometries, and so we approximate the boundary by a series of short straight lines. Because the calculations are not complicated a large number of boundary lines can be used to approximate smooth curves.

If the boundary in 3 dimensional space consists of straight lines which meet at 'kinks' where their directions change, then the straight lines map to geodesics ($k_{\mathrm{g}}=0$) and

$$\Omega=2\pi-\sum_i\alpha_i \tag{4}$$

where α_i is the angle between two lines as seen on the surface of the unit sphere. This is equal to the angle between the two planes defined by the centre of the unit sphere and each of the two straight line elements. Because the integration is very difficult for any curve beyond points on the axis of a circle, a curve is approximated by a series of straight lines and Ω is calculated numerically using the summation (4).

Fig. 6 shows three consecutive points $\mathbf{p}_{i-1}$, $\mathbf{p}_i$ and $\mathbf{p}_{i+1}$ on the boundary joined by straight lines and **r** is the point in space or apex at which we want to calculate the solid angle. We thus have two plane triangles with corners $\left(\mathbf{p}_{i-1}\mathbf{p}_i\mathbf{r}\right)$ and $\left(\mathbf{p}_i\mathbf{p}_{i+1}\mathbf{r}\right)$ and the angle α_i is given by

$$\sin\alpha_i=\frac{\left[\left(\mathbf{a}_i\times\mathbf{v}_i\right)\times\left(\mathbf{b}_i\times\mathbf{v}_i\right)\right]\cdot\mathbf{v}_i}{|\mathbf{a}_i\times\mathbf{v}_i|\,|\mathbf{b}_i\times\mathbf{v}_i|\,|\mathbf{v}_i|},$$

in which

$$\begin{aligned}\mathbf{a}_i&=\mathbf{p}_i-\mathbf{p}_{i-1}\\ \mathbf{b}_i&=\mathbf{p}_{i+1}-\mathbf{p}_i=\mathbf{a}_{i+1}\\ \mathbf{v}_i&=\mathbf{r}-\mathbf{p}_i\\ \mathbf{w}_i&=\mathbf{r}-\mathbf{p}_{i+1}=\mathbf{v}_{i+1}\\ \mathbf{u}_i&=\mathbf{r}-\mathbf{p}_{i-1}=\mathbf{v}_{i-1}.\end{aligned} \tag{5}$$

This follows from the fact that $\frac{\mathbf{a}_i \times \mathbf{v}_i}{|\mathbf{a}_i \times \mathbf{v}_i|}$ is a unit vector normal to the plane containing $\mathbf{p}_{i-1}$, $\mathbf{p}_i$ and $\mathbf{r}$, and $\frac{\mathbf{b}_i \times \mathbf{v}_i}{|\mathbf{b}_i \times \mathbf{v}_i|}$ is a unit vector normal to the plane containing $\mathbf{p}_i$, $\mathbf{p}_{i+1}$ and $\mathbf{r}$. Therefore $\frac{(\mathbf{a}_i \times \mathbf{v}_i) \times (\mathbf{b}_i \times \mathbf{v}_i)}{|\mathbf{a}_i \times \mathbf{v}_i|\,|\mathbf{b}_i \times \mathbf{v}_i|}$ is a vector in the direction of $\mathbf{v}_i$ whose magnitude is the sine of the angle between the two planes.

Using the properties of the vector triple product and the scalar triple product,

$$\begin{aligned}\sin\alpha_i &= \frac{[\mathbf{v}_i \times (\mathbf{a}_i \times \mathbf{v}_i)] \cdot (\mathbf{b}_i \times \mathbf{v}_i)}{|\mathbf{a}_i \times \mathbf{v}_i|\,|\mathbf{b}_i \times \mathbf{v}_i|\,|\mathbf{v}_i|} = \frac{[(\mathbf{v}_i \cdot \mathbf{v}_i)\,\mathbf{a}_i - (\mathbf{a}_i \cdot \mathbf{v}_i)\,\mathbf{v}_i] \cdot (\mathbf{b}_i \times \mathbf{v}_i)}{|\mathbf{a}_i \times \mathbf{v}_i|\,|\mathbf{b}_i \times \mathbf{v}_i|\,|\mathbf{v}_i|} \\ &= \frac{|\mathbf{v}_i|\,(\mathbf{a}_i \times \mathbf{b}_i) \cdot \mathbf{v}_i}{|\mathbf{a}_i \times \mathbf{v}_i|\,|\mathbf{b}_i \times \mathbf{v}_i|}.\end{aligned}$$

It also gives

$$\cos\alpha_i = \frac{(\mathbf{a}_i \times \mathbf{v}_i) \cdot (\mathbf{b}_i \times \mathbf{v}_i)}{|\mathbf{a}_i \times \mathbf{v}_i|\,|\mathbf{b}_i \times \mathbf{v}_i|} = \frac{(\mathbf{a}_i \cdot \mathbf{b}_i)(\mathbf{v}_i \cdot \mathbf{v}_i) - (\mathbf{a}_i \cdot \mathbf{v}_i)(\mathbf{b}_i \cdot \mathbf{v}_i)}{|\mathbf{a}_i \times \mathbf{v}_i|\,|\mathbf{b}_i \times \mathbf{v}_i|}$$

so that

$$\tan\alpha_i = \frac{|\mathbf{v}_i|\,(\mathbf{a}_i \times \mathbf{b}_i) \cdot \mathbf{v}_i}{(\mathbf{a}_i \cdot \mathbf{b}_i)(\mathbf{v}_i \cdot \mathbf{v}_i) - (\mathbf{a}_i \cdot \mathbf{v}_i)(\mathbf{b}_i \cdot \mathbf{v}_i)}. \tag{6}$$

Since we know $\sin\alpha_i$ and $\cos\alpha_i$ we can calculate α_i. However, because α_i is usually small, one should use $\sin\alpha_i$ or $\tan\alpha_i$, (6). In most practical situations α_i will lie between $-\pi$ and π. (6) gives a positive value for α_i if $\mathbf{a}_i$ and $\mathbf{b}_i$ lie in the plane of the figure in Fig. 6 and if the point $\mathbf{r}$ lies above the plane of the figure as we look at it.

5. The special case of a triangle

In the case of a boundary consisting of a triangle with straight sides, application of (4) and (6) gives (Eriksson, 1990)

$$\tan\frac{\Omega}{2} = \frac{(\mathbf{u}_i \times \mathbf{v}_i) \cdot \mathbf{w}_i}{|\mathbf{u}_i|\,|\mathbf{v}_i|\,|\mathbf{w}_i| + (\mathbf{u}_i \cdot \mathbf{v}_i)\,|\mathbf{w}_i| + (\mathbf{v}_i \cdot \mathbf{w}_i)\,|\mathbf{u}_i| + (\mathbf{w}_i \cdot \mathbf{u}_i)\,|\mathbf{v}_i|}, \tag{7}$$

where there are only 3 boundary points and $\mathbf{u}_i$, $\mathbf{v}_i$ and $\mathbf{w}_i$ are as shown in Fig. 6.

In fact to get from (4) and (6) to (7) is not a trivial task, but (7) can be proven by observing that cutting a triangle into two parts through an apex produces two triangles and demonstrating that the solid angle subtended by the full triangle is the sum of the solid angle subtended by the 2 parts.

Writing

$$\begin{aligned}\mathbf{p}_1 &= L(\cos\beta\mathbf{i} + \sin\beta\mathbf{j}) \\ \mathbf{p}_2 &= 0 \\ \mathbf{p}_3 &= L(\cos\beta\mathbf{i} - \sin\beta\mathbf{j}) \\ \mathbf{r} &= x\mathbf{i} + y\mathbf{j} + z\mathbf{k},\end{aligned}$$

where $\mathbf{i}$, $\mathbf{j}$, $\mathbf{k}$ are the standard basis vectors, and letting $L \to \infty$, so that 2 of the corners of the triangle become infinitely far away, then

$$\begin{aligned}\mathbf{u}_2 &= -L(\cos\beta\mathbf{i} + \sin\beta\mathbf{j}) \\ \mathbf{v}_2 &= x\mathbf{i} + y\mathbf{j} + z\mathbf{k} \\ \mathbf{w}_2 &= -L(\cos\beta\mathbf{i} - \sin\beta\mathbf{j})\end{aligned}$$

so that

$$\tan\frac{\Omega}{2} = \frac{2\cos\beta\sin\beta z}{\sqrt{x^2+y^2+z^2}\,(1+\cos^2\beta-\sin^2\beta) - (x\cos\beta - y\sin\beta) - (x\cos\beta + y\sin\beta)}$$

which produces

$$x^2 + y^2 + z^2 = \frac{1}{\cos^2\beta}\left(\frac{\sin\beta z}{\tan\frac{\Omega}{2}} + x\right)^2. \tag{8}$$

This is the equation of a cone with an elliptic cross-section whose shape depends on the constants Ω and β.

Thus for any boundary shape, in the immediate region of any sharp corner the surface is locally equivalent to a cone with an elliptic cross-section. Of course, without the singularity of curvature at the apex of a cone, a smooth surface must lie in the plane defined by 2 straight lines where they meet.

Allowing $\beta \to 0$ in (8) we obtain the special case of two parallel lines in which a circular cylinder replaces the elliptic cone, as we would expect from the inscribed angle theorem for a circle.

6. The gradient of the solid angle subtended by a closed curve and the Biot-Savart law

We now return again to the case of a boundary of arbitrary shape. $\nabla\Omega$ is the normal to a surface of constant Ω, see Fig. 5. To find $\nabla\Omega$ it is necessary to imagine that the point in space $\mathbf{r}$ moves slightly and all the boundary points remain fixed.

From (4),

$$\nabla\Omega = -\sum_i \nabla\alpha_i$$

and its is possible to calculate $\nabla\alpha_i$ from (6) using

$$\nabla\mathbf{v}_i = \nabla\left(\mathbf{r} - \mathbf{p}_i\right) = \nabla\mathbf{r} = \mathbf{I}$$

in which $\mathbf{I}$ is the unit tensor defined by

$$\mathbf{I}\cdot\mathbf{f} = \mathbf{f}\cdot\mathbf{I} = \mathbf{f}$$

where $\mathbf{f}$ is any vector. Thus, for example,

$$\nabla\left(\mathbf{b}_i\cdot\mathbf{v}_i\right) = \nabla\left(\mathbf{b}_i\cdot\mathbf{r}\right) = \mathbf{b}_i,$$

in which the vector $\mathbf{b}_i$ is taken as constant and only $\mathbf{r}$ and $\mathbf{v}_i$ vary.

After a not inconsiderable amount of working it is possible to obtain

$$\nabla\Omega = -\sum_i \left(\mathbf{v}_i - \mathbf{w}_i\right)\cdot\left(\frac{\mathbf{v}_i}{|\mathbf{v}_i|} - \frac{\mathbf{w}_i}{|\mathbf{w}_i|}\right)\frac{\left(\mathbf{v}_i\times\mathbf{w}_i\right)}{|\mathbf{v}_i\times\mathbf{w}_i|^2} \tag{9}$$

in which again $\mathbf{v}_i = \mathbf{r} - \mathbf{p}_i$ and $\mathbf{w}_i = \mathbf{r} - \mathbf{p}_{i+1}$ as shown in Fig. 6.

Now consider the vector $\mathbf{R}$ from a typical point on the straight line between $\mathbf{p}_i$ and $\mathbf{p}_{i+1}$ to $\mathbf{r}$. The minimum magnitude of $\mathbf{R}$ is the perpendicular distance,

$$h = \frac{|\mathbf{v}_i\times\mathbf{w}_i|}{|\mathbf{v}_i - \mathbf{w}_i|}.$$

The contribution to $\nabla\Omega$ in (9) is given by

$$\begin{aligned} -\int_{\mathbf{R}=\mathbf{v}_i}^{\mathbf{w}_i}\frac{d\mathbf{R}\times\mathbf{R}}{|\mathbf{R}|^3} &= -\frac{\mathbf{v}_i\times\mathbf{w}_i}{|\mathbf{v}_i\times\mathbf{w}_i|}\int_{\theta=\xi_i}^{\pi-\zeta_i}\frac{\sin^3\theta h d\left(h\cot\theta\right)}{h^3} \\ &= -\frac{|\mathbf{v}_i - \mathbf{w}_i|\left(\mathbf{v}_i\times\mathbf{w}_i\right)}{|\mathbf{v}_i\times\mathbf{w}_i|^2}\left(\cos\xi_i + \cos\zeta_i\right) \end{aligned} \tag{10}$$

where ξ_i and ζ_i are the angles shown in Fig. 6. It is easy to see that the final line of (10) is identical to the quantity being summed in (9).

This (apart from a multiplying constant) is the Biot-Savart law familiar from potential theory where it gives the magnetic field due to a current carrying wire in magnetostatics or the fluid velocity due to a vortex in irrotational incompressible flow of a fluid. Magnetostatics is the study of magnetic fields produced by steady currents in wires, in which our Ω would correspond to the scalar potential, when multiplied by some constant. Similarly in fluid mechanics our Ω corresponds to the velocity potential.

Note that the production of solid angle is centred on the kinks between straight line segments of boundary whereas the gradient of the solid angle is produced by each line segment separately.

For numerical evaluation we can observe that

$$\left(\mathbf{v}_i - \mathbf{w}_i\right)\cdot\left(\frac{\mathbf{v}_i}{|\mathbf{v}_i|} - \frac{\mathbf{w}_i}{|\mathbf{w}_i|}\right) = \frac{\left(|\mathbf{v}_i| + |\mathbf{w}_i|\right)}{|\mathbf{v}_i||\mathbf{w}_i|}\left(|\mathbf{v}_i||\mathbf{w}_i| - \mathbf{v}_i\cdot\mathbf{w}_i\right)$$

$$|\mathbf{v}_i\times\mathbf{w}_i|^2 = |\mathbf{v}_i|^2|\mathbf{w}_i|^2 - \left(\mathbf{v}_i\cdot\mathbf{w}_i\right)^2$$

so that we can rewrite (9) as

$$\nabla\Omega = -\sum_i \frac{\left(|\mathbf{v}_i| + |\mathbf{w}_i|\right)\left(\mathbf{v}_i \times \mathbf{w}_i\right)}{|\mathbf{v}_i|\,|\mathbf{w}_i|\left(|\mathbf{v}_i|\,|\mathbf{w}_i| + \mathbf{v}_i \cdot \mathbf{w}_i\right)} \tag{11}$$

which is more accurate when $\mathbf{v}_i$ and $\mathbf{w}_i$ are almost parallel, in which case both the numerator and denominator are very small in (9).

Equation (9) can be rewritten in other ways, such as

$$\nabla\Omega = -\sum_i \frac{\left(\mathbf{a}_i \cdot \mathbf{v}_i\right)\left(\mathbf{a}_i \times \mathbf{v}_i\right)}{|\mathbf{v}_i|\,|\mathbf{a}_i \times \mathbf{v}_i|^2} - \sum_i \frac{\left(\mathbf{b}_i \cdot \mathbf{v}_i\right)\left(\mathbf{b}_i \times \mathbf{v}_i\right)}{|\mathbf{v}_i|\,|\mathbf{b}_i \times \mathbf{v}_i|^2}, \tag{12}$$

but (11) is to be preferred for numerical work. $\mathbf{a}_i$, $\mathbf{b}_i$ and $\mathbf{v}_i$ are defined in (5).

7. Curvature of a surface of constant solid angle

We will not consider the curvature of a surface of constant solid angle in detail, although, there are various practical reasons why we should want to establish the curvature of a surface, such as structural analysis of a shell structure or the construction of a principal curvature grid on a surface. What follows is an outline of two alternatives on how one would find the curvature, but this section can be left by those only interested in establishing the surface itself, and not its curvature.

The first method utilises that $\nabla\Omega$ is normal to any surface $\Omega = \text{constant}$ and $\dfrac{\nabla\Omega}{|\nabla\Omega|}$ is the unit normal. To find the curvature of a surface we need to find how the unit normal changes direction as we move across the surface.

In order to find the gradient of $\nabla\Omega$, that is the second order tensor $\nabla\nabla\Omega$, let us use (12) and remember that as the point $\mathbf{r}$ moves only $\mathbf{v}_i$ changes, while $\mathbf{a}_i$ and $\mathbf{b}_i$ are constant. Thus

$$\begin{aligned}\nabla\nabla\Omega = &-\sum_i \left(\frac{\mathbf{a}_i}{|\mathbf{v}_i|} - \frac{\mathbf{v}_i\left(\mathbf{a}_i \cdot \mathbf{v}_i\right)}{|\mathbf{v}_i|^3}\right)\frac{\left(\mathbf{a}_i \times \mathbf{v}_i\right)}{|\mathbf{a}_i \times \mathbf{v}_i|^2} \\ &+ \sum_i \frac{\left(\mathbf{a}_i \cdot \mathbf{v}_i\right)}{|\mathbf{v}_i|}\left(\frac{\left(\mathbf{I} \times \mathbf{a}_i\right)}{|\mathbf{a}_i \times \mathbf{v}_i|^2} - \frac{2\left(\left(\mathbf{a}_i \cdot \mathbf{v}_i\right)\mathbf{a}_i - \left(\mathbf{a}_i \cdot \mathbf{a}_i\right)\mathbf{v}_i\right)\left(\mathbf{a}_i \times \mathbf{v}_i\right)}{|\mathbf{a}_i \times \mathbf{v}_i|^4}\right) \\ &\text{plus a similar expression replacing } \mathbf{a}_i \text{ by } \mathbf{b}_i\end{aligned} \tag{13}$$

in which we have used

$$\left(\mathbf{I} \times \mathbf{a}_i\right) \cdot \left(\mathbf{a}_i \times \mathbf{v}_i\right) = \mathbf{I} \cdot \left(\mathbf{a}_i \times \left(\mathbf{a}_i \times \mathbf{v}_i\right)\right) = \left(\mathbf{a}_i \cdot \mathbf{v}_i\right)\mathbf{a}_i - \left(\mathbf{a}_i \cdot \mathbf{a}_i\right)\mathbf{v}_i,$$

and

$$\begin{aligned}\mathbf{I} \times \mathbf{a}_i &= (\mathbf{ii} + \mathbf{jj} + \mathbf{kk}) \times \left(a_{i_x}\mathbf{i} + a_{i_y}\mathbf{j} + a_{i_z}\mathbf{k}\right) \\ &= -a_{i_z}(\mathbf{ij} - \mathbf{ji}) - a_{i_x}(\mathbf{jk} - \mathbf{kj}) - a_{i_y}(\mathbf{ki} - \mathbf{ik}),\end{aligned}$$

which can be found using (A.5.4) in Rubin (2000). The vectors $\mathbf{i}$, $\mathbf{j}$, $\mathbf{k}$ are the standard basis vectors.

Examination of (13) confirms that the trace of $\nabla\nabla\Omega$,

$$\nabla \cdot \nabla\Omega = \nabla^2\Omega = 0$$

so that Ω obeys Laplace's equation, as we would expect from potential theory.

We know that the second order tensor $\nabla\nabla\Omega$ in (13) must be symmetric but the quantity to be summed on the right hand side is not symmetric. One would expect that upon doing the summation the result would be symmetric.

The symmetric second order tensor

$$\beta = -\left(\mathbf{I} - \frac{\nabla\Omega\nabla\Omega}{|\nabla\Omega|^2}\right) \cdot \frac{\nabla\nabla\Omega}{|\nabla\Omega|} \cdot \left(\mathbf{I} - \frac{\nabla\Omega\nabla\Omega}{|\nabla\Omega|^2}\right)$$

tells how the direction of the unit normal varies as we move on the surface, that is in a direction perpendicular to the unit normal. β has no component normal to the surface and it is therefore a surface tensor and its components are known as the *coefficients of the second fundamental form* in differential geometry (Struik, 1961; Eisenhart, 1947; Green and Zerna, 1968).

The two principal values of β are the principal curvatures and the corresponding principal directions are the principal curvature directions. Finding the principal curvature directions is important in practice for cladding a surface with plane quadrilaterals (Pottmann et al., 2007) in which the edges of the quadrilaterals follow the principal curvature directions.

The second alternative, used to produce the principal curvature lines in the figures in §9, requires a mesh in comparison to the previous method. For each mesh face it is possible to find a quadratic for z in x and y,

$$z = ax^2 + 2bxy + cy^2 + fx + gy + h, \tag{14}$$

which passes through the six points $\mathbf{p}_i\left(x_i, y_i, z_i\right)$, $i = 0$ to 5, see Fig. 7. Having found the constants of the quadratic in (14) it is straightforward to compute the principal curvature directions by solving the eigenvectors in (15).

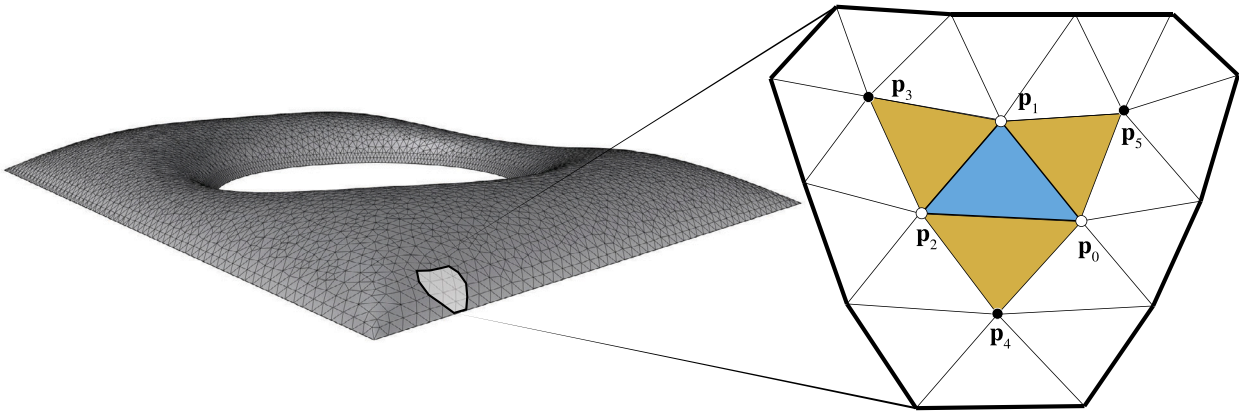

Fig. 7. It is possible to estimate the curvature of the region corresponding to the centre triangle of the surface passing through the points $\mathbf{p}_i\left(x_i, y_i, z_i\right)$, $i = 0$ to 5 by solving the quadratic (14).

$$\left[\begin{bmatrix} \frac{\partial^2 z}{\partial x^2} & \frac{\partial^2 z}{\partial x \partial y} \\ \frac{\partial^2 z}{\partial y \partial x} & \frac{\partial^2 z}{\partial y^2} \end{bmatrix} - \lambda \begin{bmatrix} 1+\left(\frac{\partial z}{\partial x}\right)^2 & \frac{\partial z}{\partial x}\frac{\partial z}{\partial y} \\ \frac{\partial z}{\partial y}\frac{\partial z}{\partial x} & 1+\left(\frac{\partial z}{\partial y}\right)^2 \end{bmatrix}\right]\begin{bmatrix} v_x \\ v_y \end{bmatrix} \tag{15}$$

8. Multiple boundaries

The current in a single wire must have the same magnitude at all points, and the same applies to the strength of a single vortex. Thus with a single wire the solid angle subtended by the wire at any point is some constant times the scalar potential. If we have more than one wire then we have to include the value of the current since it is possible to have different electric currents, or their equivalents, in the different wires. It is also possible to apply Kirchhoff's current law where sections of boundary meet.

Then (2) becomes

$$\Omega = \sum_w I_w \left(2\pi - \oint_{\partial M_w} k_g ds\right) \tag{16}$$

in which the contributions of the different parts of the boundary are weighted by the currents I_w in each of the wires w. Note that in applying Kirchhoff's current law we think of each wire w being a closed loop and along certain lengths two or more wires may run alongside each other in which case the combined current is the sum of the individual current loops, which may be positive or negative.

Changing the sign of I_w reverses the current, which should have exactly the same effect as reversing the direction of the integral $\oint_{\partial M_w} k_g ds$. However, we then have to be careful to take into account what happens to the 2π in (16). To get over this, it is often better to get rid of the 2π and instead use

$$\Omega = -\sum_w \left(I_w \oint_{\partial M_w} k_g ds\right)$$

to define our constant Ω surface. Even so we have to be aware that there is an uncertainty of 4π in each integral $\oint_{\partial M_w} k_g ds$.

9. Examples

There are few analytical solutions of constant solid angle surfaces to compare with a numerical implementation. However, as described at the end of §5 a boundary consisting of two infinitely long parallel lines produces circular surfaces of constant solid angle. This is the equivalent to the lines of constant velocity potential produced by two infinite straight parallel equal and opposite line vortices (Lamb, 1932). We used a long thin rectangle to produce Fig. 8, where the blue curves are indeed circles.

On a circular boundary, as in Fig. 9, the shape is not a sphere since it is more flat on the top with increasing curvature near the boundary. The shape is more similar to a water droplet on a flat surface deformed by gravity than a sphere.

Figs. 10 and 11 have the same boundary curves as the surface in Fig. 4, three circles with different radius in the same plane, and the red and blue curves follows the principal curvature lines. In Fig. 11 one can see in the zoomed in areas that the principal curvature directions follow the surface boundary, thus confirming that the slope is constant along the boundary.

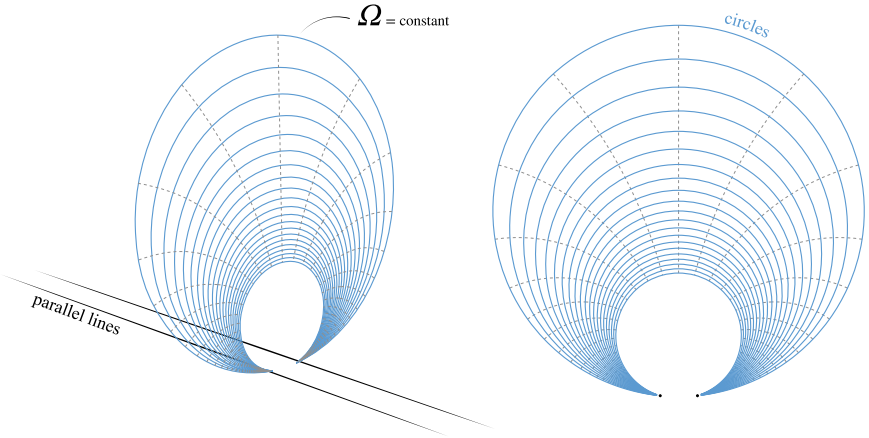

Fig. 8. Potential flow produced by two straight parallel equal and opposite vortices modelled by a long rectangle using our method.

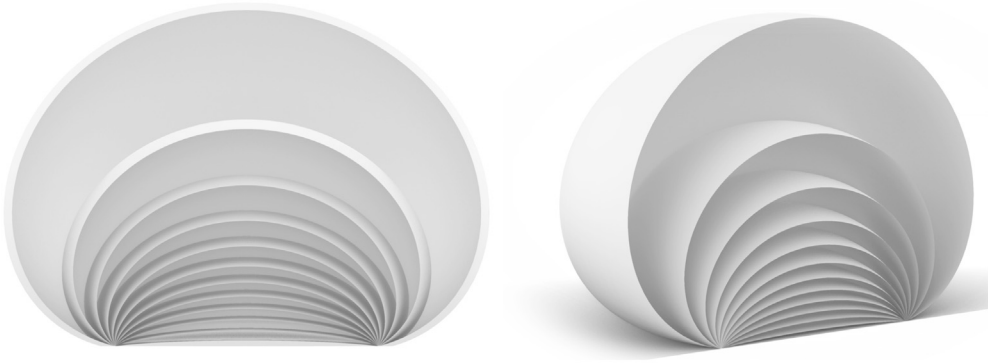

Fig. 9. Surfaces with different constant solid angles on a circular boundary.

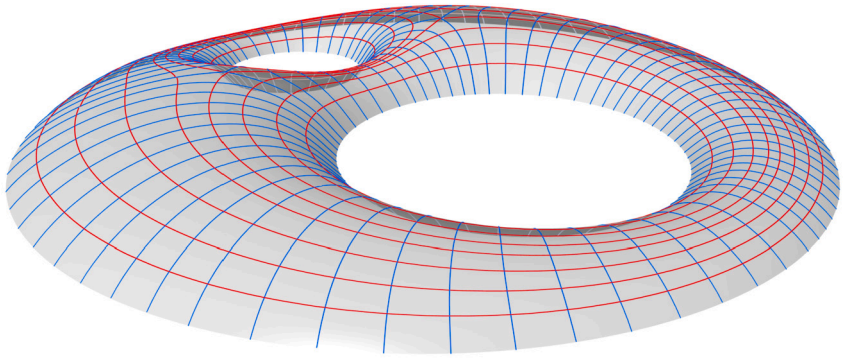

Fig. 10. Elevation of surface with constant solid angle having the same boundary curves as Figs. 4 and 11, three circles with varying diameter that lies the same plane. The red and blue curves follow the principal curvature directions.

In Figs. 12 to 14 we have chosen the same boundary curves as the British Museum Great Court roof (Williams, 2001) (Fig. 1(a)) and placed them in the same plane. The principal curvature lines follow both the circular and the rectangular boundaries. Only in the close proximity of the corners can one see that the principal curvature directions diverge towards the corner.

Figs. 15 to 17 are all the same surface whose three boundary curves lie in the same plane. The boundary conditions were chosen to be quite problematic, but even so, the slope is constant along the boundary curves with a fine mesh.

The surfaces in Figs. 18 and 19 have the same boundary curves, a rectangular exterior curve and a circular interior curve. Because the two boundary curves are at different levels, the slope around each curve will not be constant. Nevertheless we can rotate the slope around each curve independently by varying the current in the equivalent wire.

The relative height difference of the interior curve between Fig. 18 (a) and Fig. 18 (b) makes the slope at the exterior curve either positive or negative. Thus, Fig. 18 (a) and Fig. 19 (a) are reminiscent of the umbrella shells by Felix Candela and Amancio Williams

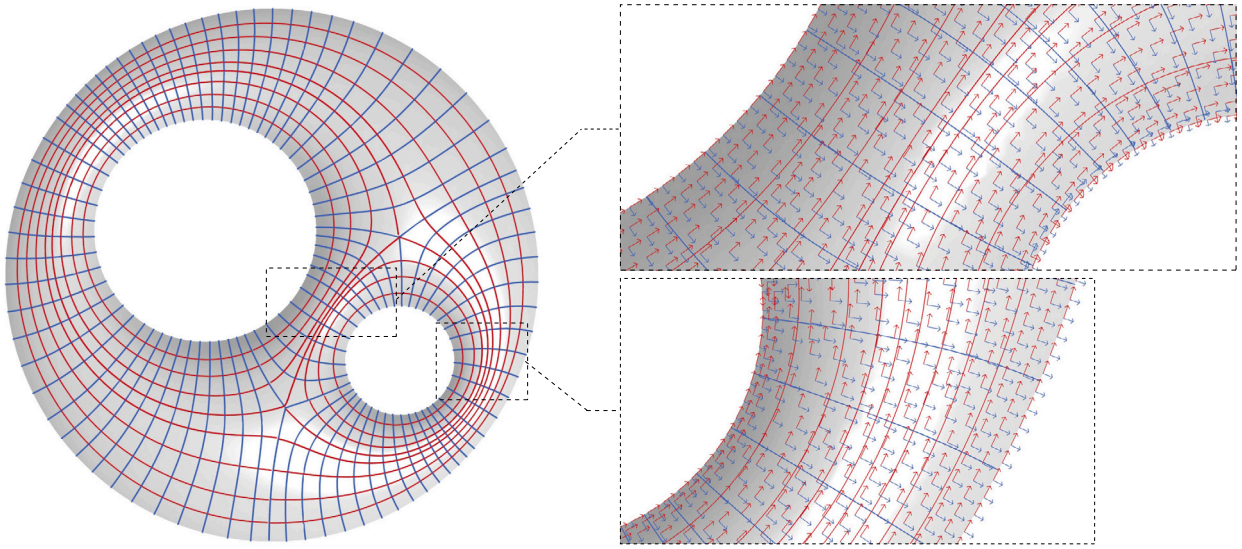

Fig. 11. Top view of surface with constant solid angle having the same boundary curves as Figs. 4 and 10. Red and blue curves follows the principal curvature directions. Two areas are zoomed in to highlight that the principal curvature directions, seen as vectors, follow the surface boundary.

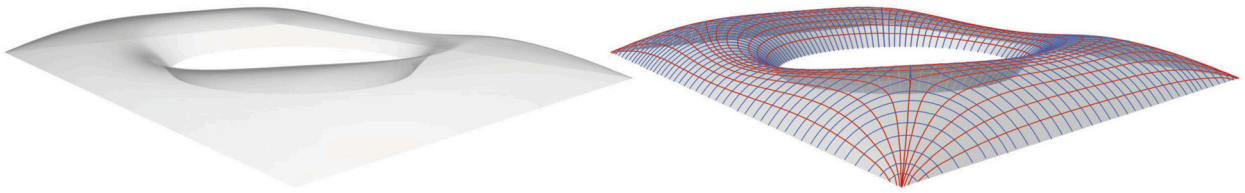

Fig. 12. Elevation of surface with constant solid angle having the same boundary curves as the British Museum Great Court roof. It is the same surfaces as seen in Figs. 13 and 14.

(Rian and Sassone, 2014), while Fig. 18 (b) and Fig. 19 (b) resemble the shape of the British Museum Great Court roof. Changing the value of the solid angle will not make the slope change from positive to negative as seen in Figs. 20 (a) to (c), unless breaking the surface into two.

The phenomenon of surface separation is illustrated in Fig. 21 using points rather than a mesh and the same boundary conditions as Fig. 18 (a). One can see the surface as one in Fig. 21 (a) but by changing the constant solid angle gradually one can see the surface starting to separate in Figs. 21 (b) to (c). By further changing the solid angle the surface separate completely into two independent surfaces in Fig. 21 (d), both having the same constant solid angle.

Figs. 22 to 24 have a similar geometry to that in Fig. 19, but with several spans to model a potential bridge design. It is also possible to rotate the boundary curves as shown in Figs. 25 and 26.

10. Conclusions and future work

Constant solid angle surfaces enable one to control the boundary slope of a shell structure and hence achieve an approximately constant span-to-height ratio as the span varies. They also allow a principal curvature net to meet a plane boundary without cutting quadrilaterals, as shown in Figs. 11 and 13. This means one can get a structurally viable shell also suitable for surface grids with planar panels.

The constant boundary slope could also be used in the choice of Airy stress function where the constant slope would give a shell where the forces are concentrated at the corners of a boundary consisting of straight lines. This could be useful in projects with a similar context as the British Museum Great Court roof where forces are directed towards the corners relieving the walls from lateral thrust.

We have made no attempt to optimise the surfaces from the structural point of view, which depends both upon the shape of the surface and its boundary support (Green and Zerna, 1968). However, the conical shape at a boundary kink can be advantageous if there is a concentrated thrust at the kink, and that is the reason for the conical corners of the British Museum Great Court roof.

The method could easily be adapted so that the required solid angle is no longer a constant, but some given function of the x, y, z coordinates in space. Thus, if we were dissatisfied with the shape of the surfaces on a circular boundary in Fig. 9, we could specify the solid angle as a function of z or $\sqrt{x^2+y^2}$, which would preserve the rotational symmetry. In order to do this we would need to include the gradient of the required solid angle alongside the gradient in the solid angle.

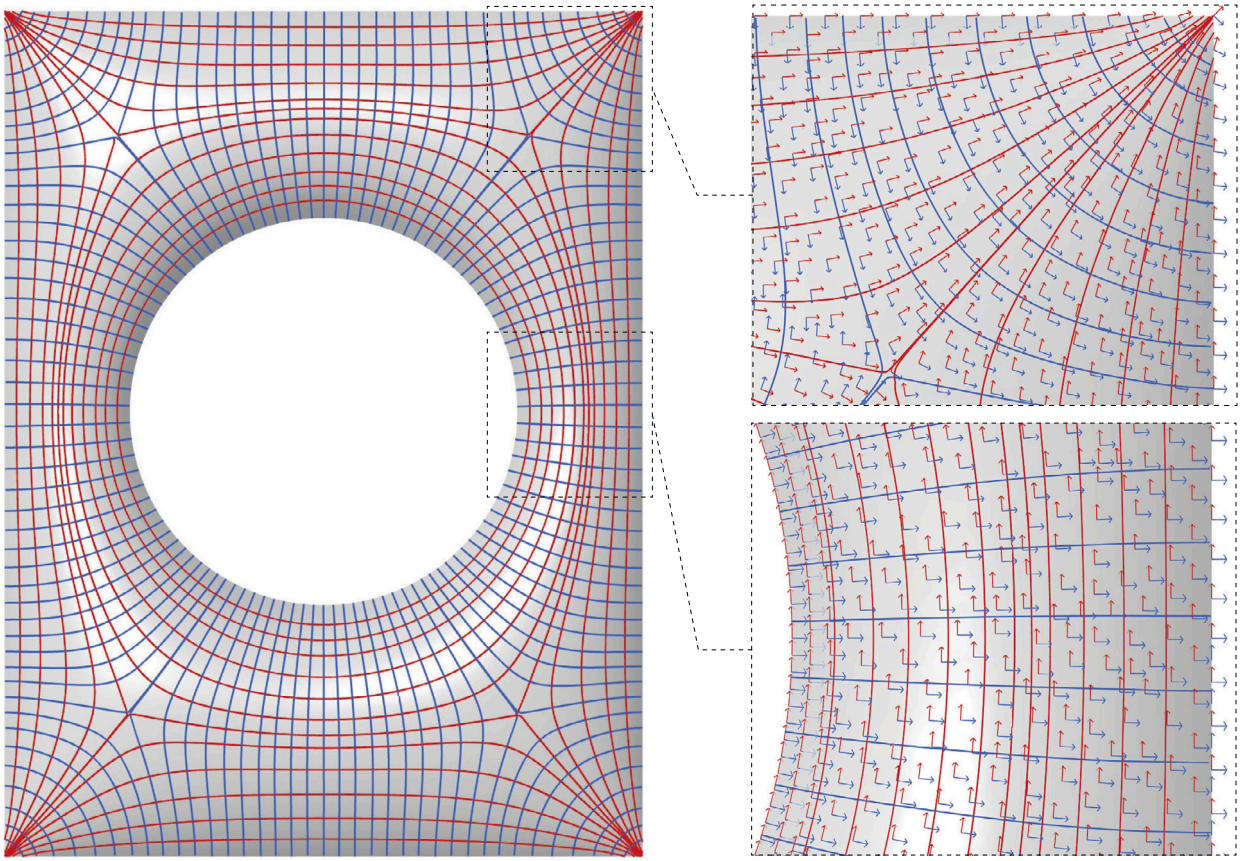

Fig. 13. Top view of the same surfaces seen in Figs. 12 and 14. The red and blue curves are the principal curvature lines. Two areas are zoomed in to highlight that the principal curvature directions, seen as vectors, follow the surface boundary.

Fig. 14. Elevation of surface with constant solid having the same boundary curves as the British Museum Great Court roof. It is the same surfaces as in seen in Figs. 12 and 13. The material is transparent to visualise the interior space.

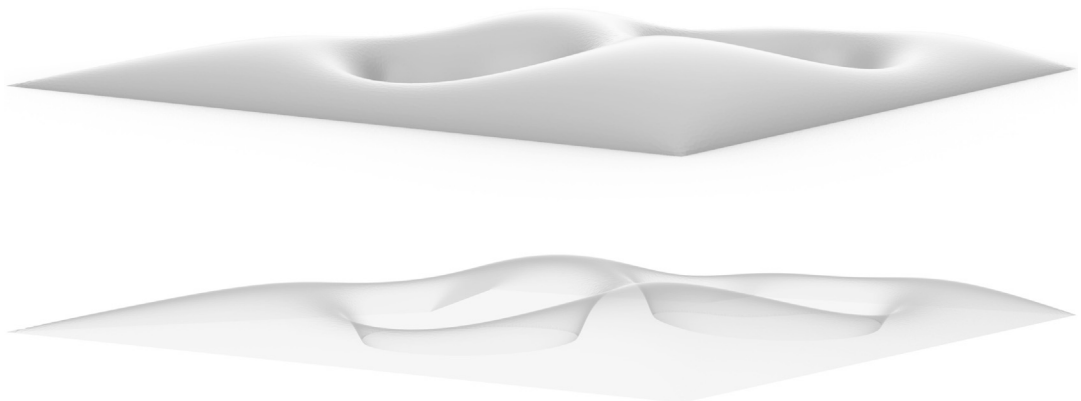

Fig. 15. Perspective views of the constant solid angle surface in Figs. 16 and 17. The slope is constant around each boundary, but varies from boundary to boundary.

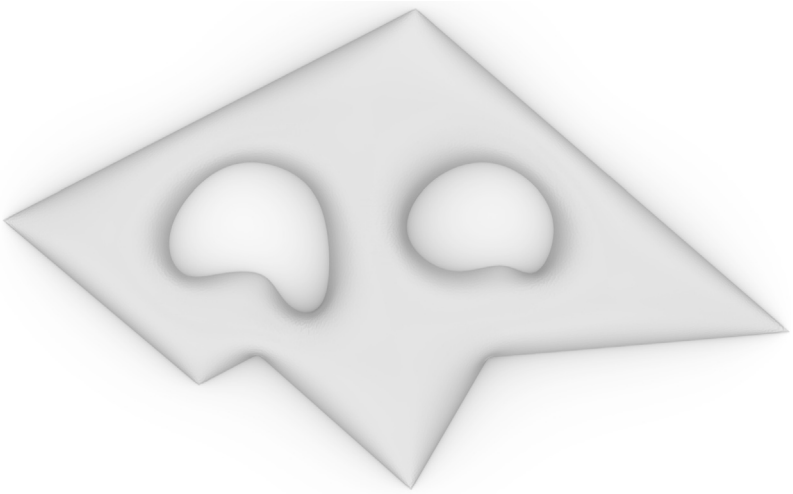

Fig. 16. Top view of the surface seen in Figs. 15 and 17.

Fig. 17. Elevation of the surface in Figs. 15 and 16. The material is transparent to visualise the interior space.

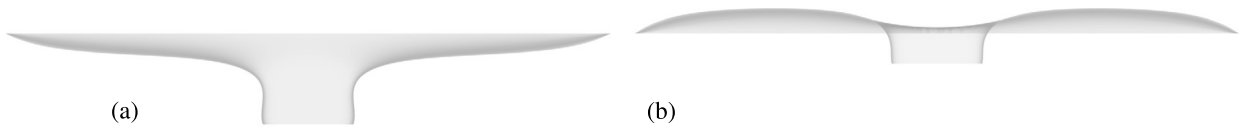

Fig. 18. Elevation of two surfaces with the same boundary curves, a rectangle and a circle which is lowered in relation to rectangle. In (a) the circle is placed lower than that in (b).

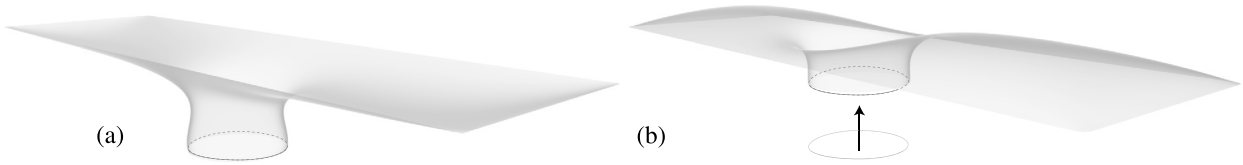

Fig. 19. Perspective view of the same geometry as in Figs. 18 (a) and 18 (b) rendered with a transparent material.

It is possible to generate surfaces having multiple complex boundary curves positioned and angled in different planes with individually tuned currents in the wires. One drawback is that the principal curvatures no longer follow the boundary curves. However, it is possible to rotate the slope around each curve independently by varying the current in the equivalent wire. Thus, the shapes can still be useful, and they can be used for other surface grids and possibly in other fields where one needs to generate surfaces without an initial mesh. However, there is still much to learn about the properties of constant solid angle surfaces. Having curves in different positioned and inclined planes as in Figs. 25 and 26 it can be challenging to tune the parameters and find good initial positions for the points. Hence, further development of the technique can be done for such situations.

CRediT authorship contribution statement

Emil Adiels: Conceptualization, Methodology, Software, Visualization, Writing – original draft, Writing – review & editing. **Mats Ander:** Conceptualization, Supervision, Writing – original draft, Writing – review & editing. **Chris J.K. Williams:** Conceptualization, Formal analysis, Methodology, Supervision, Writing – original draft, Writing – review & editing.

Declaration of competing interest

The authors declare the following financial interests/personal relationships which may be considered as potential competing interests: Emil Adiels reports financial support was provided by Chalmers University of Technology Foundation. Emil Adiels reports

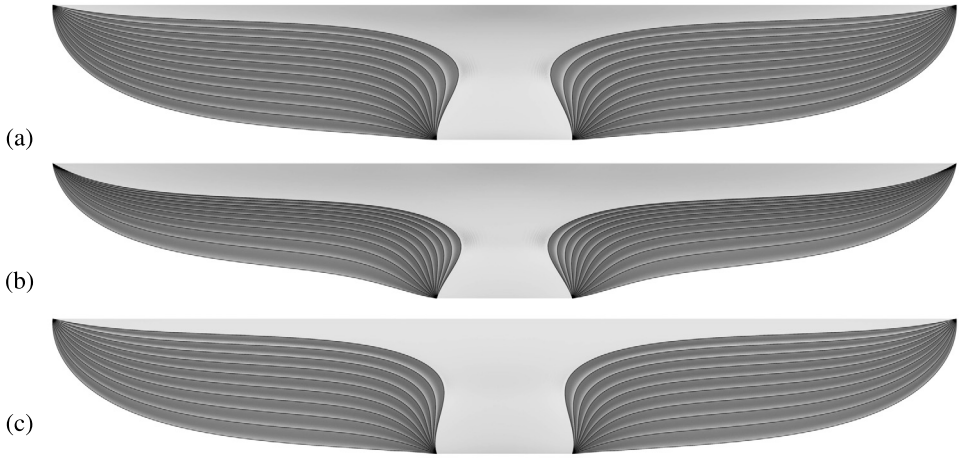

Fig. 20. These three sections illustrate the effect of varying the solid angle and the ratio of the current in the circular and rectangular wires. The boundary conditions are the same as in Fig. 18 (a). In (a) the value of the solid angle varies while the current is the same in both wires. In (b) the current in the rectangular wire is varying for a value of constant solid angle, while in (c) the current in the circular wire is varying.

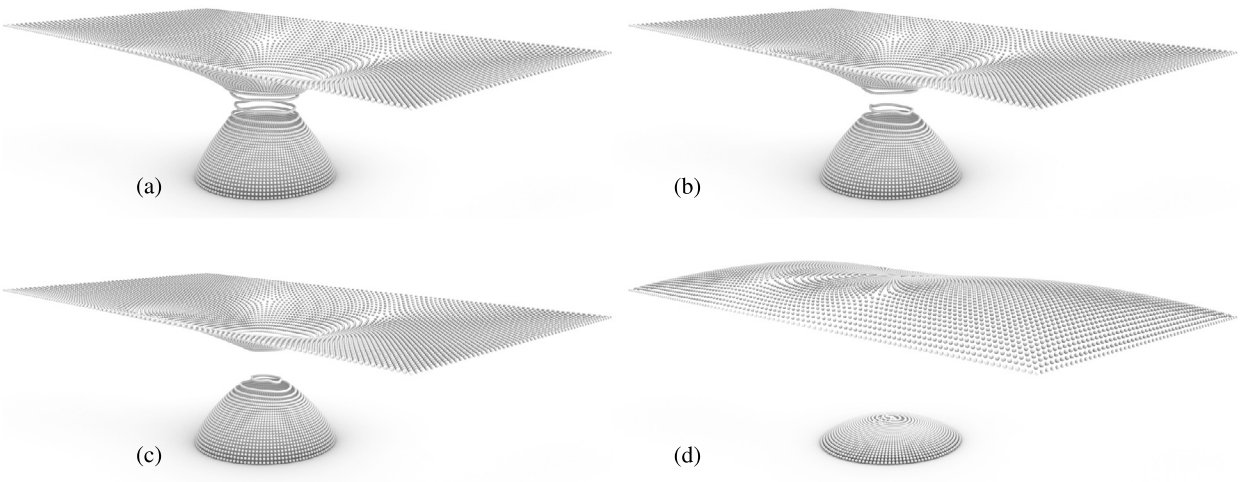

Fig. 21. Surfaces are represented by points with varying values of solid angle. The boundary curves are the similar to Fig. 18 (a), a rectangle and a circle in horizontal planes at different levels. At a certain value of the constant solid angle, the surface in (a) starts to separate into two surfaces seen in (b) and (c). In (d) the surface is split in two surfaces, both having the same constant solid angle.

Fig. 22. Perspective of a bridge design with a constant solid angle surface.

Fig. 23. Elevation of a bridge design with a constant solid angle surface.

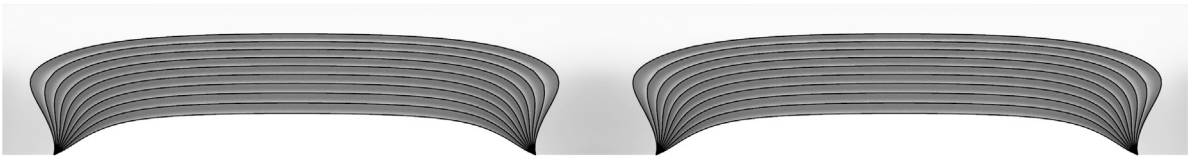

Fig. 24. Longitudinal sections of bridge designs with varying value of solid angle.

Fig. 25. It is possible to have boundary curves that lie in differently angled planes.

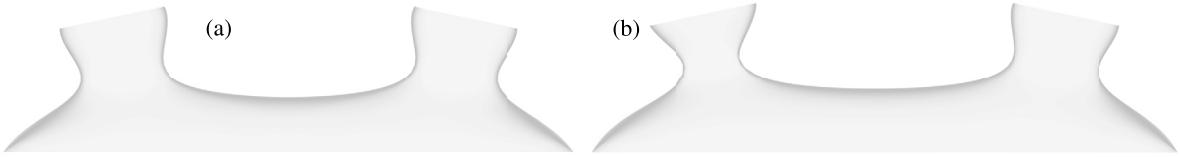

Fig. 26. Elevations of two surfaces sharing the same boundaries as in Fig. 25. In (a) the currents in the two circular wires are equal, in (b) they are different.

financial support was provided by Digital Twin Cities Centre, Chalmers University of Technology (Vinnova, grant number: 2019-00041).

Data availability

No data was used for the research described in the article.

Acknowledgements

We greatly appreciate the financial support from the Chalmers University of Technology Foundation and the Digital Twin Cities Centre (Vinnova, grant number: 2019-00041). We would also like to thank Daniel Piker for making us aware of the work regarding surfaces associated with knotted fields of by for instance Machon and Alexander (2013); Binysh and Alexander (2018); Binysh (2019). We are thankful for the helpful comments from Prof. Klas Modin. Furthermore, we would like to thank Berlin Zoo for giving us the kind permission to use their picture from the Hippo House.

References

Adiels, E., Williams, C.J.K., 2021. The construction of new masonry bridges inspired by Paul Séjourné. In: IASS Annual Symposium and Spatial Structures Conference: Inspiring the Next Generation. Guildford, Surrey.

Adiels, E., Ander, M., Williams, C.J.K., 2017. Brick patterns on shells using geodesic coordinates. In: IASS Annual Symposium 2017 “Interfaces: Architecture.engineering.science”, pp. 1–10.

Adriaenssens, S., Ney, L., Bodarwe, E., Williams, C., 2012. Finding the form of an irregular meshed steel and glass shell based on construction constraints. J. Archit. Eng. 18 (3), 206–213. https://doi.org/10.1061/(ASCE)AE.1943-5568.0000074.

Adriaenssens, S., Block, P., Veenendaal, D., Williams, C., 2014. Shell Structures for Architecture: Form Finding and Optimization. Routledge. ISBN 9781315849270.

Allen, E., 2003. Guastavino, Dieste, and the two revolutions in masonry vaulting. In: Anderson, S. (Ed.), Eladio Dieste: Innovation in Structural Art, 1st ed. Princeton Architectural Press, New York. ISBN 9781616890025.

Binysh, J., 2019. Construction and dynamics of knotted fields in soft matter systems. Ph.D. thesis. University of Warwick. http://wrap.warwick.ac.uk/145928.

Binysh, J., Alexander, G.P., 2018. Maxwell’s theory of solid angle and the construction of knotted fields. J. Phys. A, Math. Theor. 51. https://doi.org/10.1088/1751-8121/aad8c6.

Bobenko, A.I., Schröder, P., 2005. Discrete Willmore flow. In: ACM SIGGRAPH 2005 Courses, SIGGRAPH ’05. Association for Computing Machinery, New York, NY, USA. ISBN 9781450378338, pp. 5–es.

Chebyshev, P.L., 1946. On the cutting of garments. Usp. Mat. Nauk 1 (2(12)), 38–42.
Collins, G.R., 1963. Antonio Gaudi: structure and form. Perspecta 8, 63–90.
Crane, K., de Goes, F., Desbrun, M., Schröder, P., 2013. Digital geometry processing with discrete exterior calculus. In: ACM SIGGRAPH 2013 Courses, SIGGRAPH '13. ACM, New York, NY, USA.
Eisenhart, L.P., 1947. An Introduction to Differential Geometry, with Use of the Tensor Calculus. Princeton University Press.
Eriksson, F., 1990. On the measure of solid angles. Math. Mag. 63 (3), 184–187. http://www.jstor.org/stable/2691141.
Faber, C., 1963. Candela: The Shell Builder. Reinhold Publishing Corporation. https://catalog.hathitrust.org/Record/000452039.
Green, A.E., Zerna, W., 1968. Theoretical Elasticity, 2nd ed. Oxford University Press.
Huerta, S., 2006. Structural design in the work of Gaudí. Archit. Sci. Rev. 49 (4), 324–339. https://doi.org/10.3763/asre.2006.4943.
Joachimsthal, F., 1846. Demonstrationes theorematum ad superficies curvas spectantium. J. Reine Angew. Math. 30, 347–350. https://doi.org/10.1515/crll.1846.30.347.
Klaus, B., Berthold, B., Frei, O., 1987. Seifenblasen - Forming Bubbles, IL 18. Institut für Leichte Flächentragwerke. ISBN 3-7828-2018-5.
Lamb, H., 1932. Hydrodynamics, 6th ed. Cambridge University Press.
Liddell, I., 2015. Frei Otto and the development of gridshells. Case Stud. Struct. Eng. 4, 39–49. https://doi.org/10.1016/j.csse.2015.08.001.
Lorensen, W.E., Cline, H.E., 1987. Marching cubes: a high resolution 3d surface construction algorithm. In: Proceedings of the 14th Annual Conference on Computer Graphics and Interactive Techniques, SIGGRAPH 1987, vol. 21, pp. 163–169.
Machon, T., Alexander, G.P., 2013. Knotted Nematics. http://arxiv.org/abs/1307.6819. arXiv:1307.6819.
Miki, M., Igarashi, T., Block, P., 2015. Parametric self-supporting surfaces via direct computation of Airy stress functions. ACM Trans. Graph. 34 (4). https://doi.org/10.1145/2766888.
Miki, M., Adiels, E., Baker, W., Mitchell, T., Sehlström, A., Williams, C.J., 2022. Form-finding of shells containing both tension and compression using the Airy stress function. Int. J. Space Struct. https://doi.org/10.1177/09560599221102618.
Müller, S., Röger, M., 2014. Confined structures of least bending energy. J. Differ. Geom. 97 (1), 109–139. https://doi.org/10.4310/jdg/1404912105.
Pellis, D., Pottmann, H., 2018. Aligning principal stress and curvature directions. In: Advances in Architectural Geometry 2008, pp. 34–53.
Pellis, D., Kilian, M., Pottmann, H., Pauly, M., 2021. Computational design of Weingarten surfaces. ACM Trans. Graph. 40 (4). https://doi.org/10.1145/3450626.3459939.
Pottmann, H., Wallner, J., 2017. Freeform architecture and discrete differential geometry. In: Kropatsch, W.G., Artner, N.M., Janusch, I. (Eds.), Discrete Geometry for Computer Imagery. Springer International Publishing, Cham. ISBN 978-3-319-66272-5, pp. 3–8.
Pottmann, H., Brell-Cokcan, S., Wallner, J., 2007. Discrete surfaces for architectural design. In: Chenin, P., Lyche, T., Schumaker, L.L. (Eds.), Curves and Surface Design: Avignon 2006. Nashboro Press. ISBN 978-0-9728482-7-5, pp. 213–234.
Pottmann, H., Eigenzatz, M., Vaxman, A., Wallner, J., 2014. Architectural geometry. Comput. Graph., 1–22. https://doi.org/10.1680/stbu.9.00088.
Rian, I.M., Sassone, M., 2014. Tree-inspired dendriforms and fractal-like branching structures in architecture: a brief historical overview. Front. Archit. Res. 3. https://doi.org/10.1016/j.foar.2014.03.006.
Rubin, M., 2000. Cosserat Theories: Shells, Rods and Points. Springer Science+Business Media Dordrecht. ISBN 978-94-015-9379-3.
Rubió i Bellver, J., 1913. Dificultats per a arribar a la sintessis arquitectònica. In: Anuario de la Asociación de Arquitectos de Cataluña, pp. 63–79.
Sadowsky, M.A., Sternberg, E., 1950. Elliptic integral representation of axially symmetric flows. Q. Appl. Math. 8 (2), 113–126. http://www.jstor.org/stable/43633799.
Schek, H.J., 1974. The force density method for form finding and computation of general networks. Comput. Methods Appl. Mech. Eng. 3 (1), 115–134. https://doi.org/10.1016/0045-7825(74)90045-0.
Schlaich, J., Schober, H., 1996. Glass-covered grid-shells. Struct. Eng. Int. J. Int. Assoc. Bridge Struct. Eng. 6 (2), 88–90. https://doi.org/10.2749/101686696780495716.
Schlaich, J., Schober, H., 2005. Freeform glass roofs. In: Structures Congress 2005, pp. 25–27.
Stoker, J.J., 1969. Differential Geometry. Wiley-Interscience, New York.
Struik, D.J., 1961. Lectures on Classical Differential Geometry. Addison-Wesley.
Tellier, X., Douthe, C., Hauswirth, L., Baverel, O., 2019. Linear Weingarten surfaces for conceptual design. In: Proceedings of the International Fib Symposium on Conceptual Design of Structures, pp. 225–232.
Timoshenko, S., Woinowsky-Krieger, S., 1959. Theory of Plates and Shells, 2nd ed. McGraw-Hill.
Van Oosterom, A., Strackee, J., 1983. The solid angle of a plane triangle. IEEE Trans. Biomed. Eng. BME-30 (2), 125–126. https://doi.org/10.1109/TBME.1983.325207.
Weisstein, E.W., n.d. From MathWorld—A Wolfram Web Resource. https://mathworld.wolfram.com/SolidAngle.html (last visited on 2023 08 15).
Williams, C.J.K., 1980. Form finding and cutting patterns for air-supported structures. In: Air-Supported Structures: the State of the Art. Institution of Structural Engineers, London, pp. 99–120.
Williams, C.J.K., 1987. Use of structural analogy in generation of smooth surfaces for engineering purposes. Comput. Aided Des. 19 (6), 310–322.
Williams, C.J.K., 2001. The analytic and numerical definition of the geometry of the British Museum Great Court roof. In: Burry, M., Datta, S., Dawson, A., Rollo, A. (Eds.), Mathematics & Design 2001. Deakin University, Geelong, Australia, pp. 434–440.
Wright, D.T., 1965. Membrane forces and buckling in reticulated shells. J. Struct. Div. 91 (1), 173–201. https://doi.org/10.1061/JSDEAG.0001205.
Zienkiewicz, O.C., Taylor, R.L., 1991. The Finite Element Method, Fourth Edition, Volume 2: Solid and Fluid Mechanics, Dynamics and Non-linearity, 4th ed.